Experimental observation of Dyakonov plasmons in the mid-infrared

Takayama, Osamu; Dmitriev, P.; Shkondin, Evgeniy; Yermakov, O.; Panah, M.; Golenitskii, K.; Jensen, F.; Bodganov, A.; Lavrinenko, Andrei

Published in:
Semiconductors

Link to article, DOI:
10.21883/FTP.2018.04.45814.03

Publication date:
2018

Document Version
Peer reviewed version

ISSN 1063-7826, Semiconductors, 2018, Vol. 52, No. 4, pp. 442–446. © Pleiades Publishing, Ltd., 2018.

XXV INTERNATIONAL SYMPOSIUM
"NANOSTRUCTURES: PHYSICS AND TECHNOLOGY",
SAINT PETERSBURG, JUNE 26–30, 2017.
OPTOELECTRONICS, OPTICAL PROPERTIES

Experimental Observation of Dyakonov Plasmons in the Mid-Infrared[1]

O. Takayama[a], P. Dmitriev[b], E. Shkondin[a, c], O. Yermakov[b], M. Panah[b], K. Golenitskii[d], F. Jensen[c], A. Bogdanov[b, d]*, and A. Lavrinenko[a, b]

[a] *DTU Fotonik—Department of Photonics Engineering, Technical University of Denmark, Kgs. Lyngby, DK-2800 Denmark*
[b] *Department of Nanophotonics and Metamaterials, ITMO University, St. Petersburg, 197101 Russia*
[c] *DTU Danchip—National Center for Micro- and Nanofabrication, Technical University of Denmark, Kgs. Lyngby, DK-2800 Denmark*
[d] *Ioffe Institute, St. Petersburg, 194021 Russia*
**e-mail: bogdanov@mail.ioffe.ru*
Received December 25, 2017

Abstract—In this work, we report on observation of Dyakonov plasmons at an interface with a hyperbolic metamaterial in the mid-IR. The hyperbolic metamaterial is implemented as a CMOS-compatible high aspect ratio grating structure with aluminium-doped ZnO (AZO) ridges grown by atomic layer deposition in deep trench silicon matrix. The dispersion of Dyakonov plasmons is characterized by the attenuated total reflection method in the Otto configuration. We demonstrate that Dyakonov plasmons propagate in a broad range of directions (a few tens of degrees) in contrast to the classical Dyakonov surface waves (about one tenth of degree). The obtained results provide useful guidelines for practical implementations of structures supporting Dyakonov plasmons in the mid-IR.

DOI: 10.1134/S1063782618040279

1. INTRODUCTION

Research on surface waves (SWs) has intensified in the last decade [1–3] due to their promising applications in nanophotonics, sensing [4], light-trapping of nanoparticles [5], and near-field imaging [6]. The most studied SWs are surface plasmon-polaritons (SPPs) supported at an interfaces between metals and dielectrics [7, 8]. They were firstly observed in 1902 by R. Wood [9]. Today, a large number of studies on SPPs formed a new branch of optics—Plasmonics [7, 10, 11]. One of the main advantages of SPPs is their strong localization, providing high sensitivity to very thin layers of analytes, and making possible to squeeze optical devices up to nanoscale. The disadvantage of SPP is related to unavoidable losses that prevent SPPs propagation over long distances.

Another, relatively new, class of surface waves are Dyakonov waves (DWs) theoretically predicted in [12]. This type of surface waves can propagate along an interface of a uniaxial dielectric with permittivity tensor

$$\hat{\varepsilon} = \begin{pmatrix} \varepsilon_o & 0 & 0 \\ 0 & \varepsilon_o & 0 \\ 0 & 0 & \varepsilon_e \end{pmatrix}, \quad (1)$$

and an isotropic medium with permittivity ε. Here ε_o and ε_e stand for ordinary and extraordinary permittivities, respectively. DWs have almost no losses but they exist in a very small angular domain of directions, which is about 0.1° for natural anisotropic materials [13]. Moreover, the necessary condition for existence of Dyakonov waves

$$\varepsilon_o < \varepsilon < \varepsilon_e, \quad (2)$$

brings additional difficulties for their experimental observation and limits possible applications. Indeed, the time gap between theoretical prediction of DWs and their experimental observations is over 20 years [14, 15]. Using of artificial media facilitates the achievement of strong anisotropy and, therefore, substantially increases the range of allowed propagation directions for DWs [16]. In particular, it was shown in [17] that for hyperbolic metamaterials (HMMs) of the second type, condition (2) is fulfilled almost always since for them $\varepsilon_o < 0$ and $\varepsilon_e > 0$. In this case, the angular domain of the allowed propagation directions becomes very broad. Due to negative ε_o, the Dyakonov waves partially possess properties of SPPs. It is why DWs at interfaces of HMMs are also called Dyakonov plasmons (DPs).

Combining a SPP and DW brings new features by taking over traits from both types of surface waves.

[1] The article is published in the original.

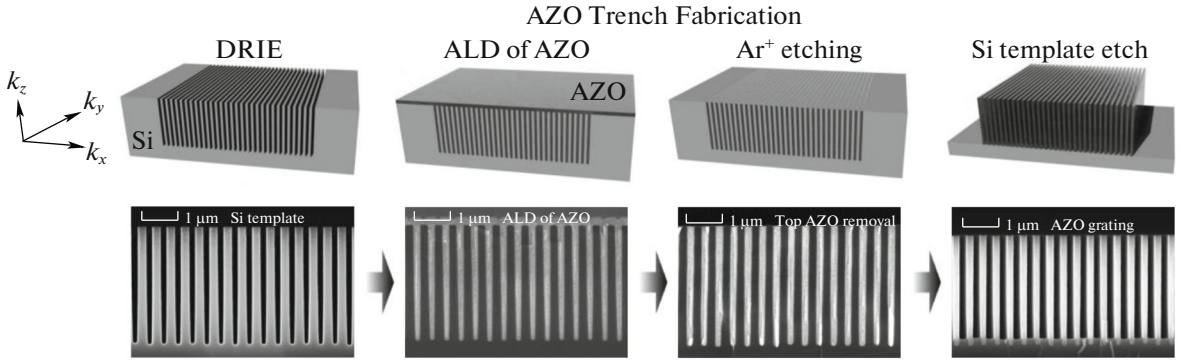

Fig. 1. Schematic of AZO trench fabrication and corresponding SEM cross section image. (First column) Realization of silicon template using deep reactive ion etching (DRIE, Bosch process). (Second column) AZO coating layer deposited by ALD on silicon template. (Third column) Removal of the top part of the AZO layer using physical Ar^+ ion sputtering. (Fourth column) Selective silicon etch (template removal) to fabricate free standing AZO trenches.

This is just the case when metamaterials can play essential roles since optical parameters not occurring in nature are often required. In spite of the fact that various types of optical HMMs have been fabricated and characterized, including multilayers [18–22], shallow metallic gratings [23, 24], and pillar structures [25–27], the DPs have been analyzed mostly theoretically.

Here, we report on the successful development of a CMOS-compatible material platform suitable for observation and operating with DPs in the mid-IR. The platform is based on conducting oxide—Al-doped ZnO (AZO) high aspect ratio trench structures, providing flexible engineering and tuning of directivity and dispersion of Dyakonov plasmons.

2. SAMPLE FABRICATION

Conducting oxides are widely used in the visible range because they are transparent and conduct electrical current [28, 29]. However, the conducting oxides are also very prospective for mid-IR applications, since they demonstrate pronounced plasmonic properties in this range [30]. In contrast to metals, the plasma frequency of conducting oxides can be efficiently tuned by changing the doping level [31].

As the first step, we deposit a 200 nm layer of AZO on a glass substrate and measure the reflectance spectrum. From this data we roughly estimate the concentration of free electrons as $7 \times 10^{20} - 8 \times 10^{20}$ cm^{-3} that corresponds to the plasma frequency around 260–280 THz. Therefore, we expect plasmonic behavior of AZO at wavelengths of several microns and higher.

Then we fabricated a CMOS-compatible AZO high aspect ratio trench structures combining atomic layer deposition (ALD) and dry etch techniques [32, 33]. The use of ALD in combination with a sacrificial Si template is a novel way to create high aspect ratio structures of metal oxides. The process starts with fabrication of a silicon trench template using deep reactive ion etching (DRIE), and the template is conformal-coated with an AZO film using ALD. The thickness of the coating should be at least half of the maximum distance between the Si trenches to fill the spacing between them. The top part of the AZO coatings can be removed by dry etching using Ar^+ ion sputtering. Then, the silicon layers can be etched away selectively by a conventional SF_6 based isotropic Si dry etch process. Figure 1 shows a scheme of the described fabrication stages and the SEM images of the resulting structure at each of the steps. This approach enables us to fabricate high-quality high aspect ratio optical metamaterials on 2×2 cm^2 or even larger areas.

To determine the effective ordinary and extraordinary dielectric permittivities of the fabricated structure in the mid-IR we measured the reflectance spectra for different polarizations of the incident wave. The effective dielectric permittivities are plotted in Fig. 2 by the solid lines. One can see that the hyperbolic regime is observed at the wavelength $\lambda > 2.5$ μm. We also fit experimental data by the well-known formula for effective parameters of a multilayer structure [34]:

$$\varepsilon_o = \xi + (1-\xi)\varepsilon_{AZO}(\omega); \quad \frac{1}{\varepsilon_e} = \xi + \frac{1-\xi}{\varepsilon_{AZO}(\omega)}. \qquad (3)$$

The blue and red circle markers in Fig. 2 resulted from fitting with Eq. (3). The fitting parameters are following: $\xi = 0.65$, $\Omega_p = 270$ THz, $\gamma = 50$ THz, $\varepsilon_\infty = 4.1$. One can see that the effective medium theory is applicable for our structure in a broad spectral range.

3. EXPERIMENTAL SETUP

A sketch of the experimental setup is shown in Fig. 3. The setup is based on an FTIR spectrometer (VERTEX 70, Bruker) equipped by a hemispherical Ge prism with the diameter 20 mm. The prism is placed on the sample with an air gap providing the

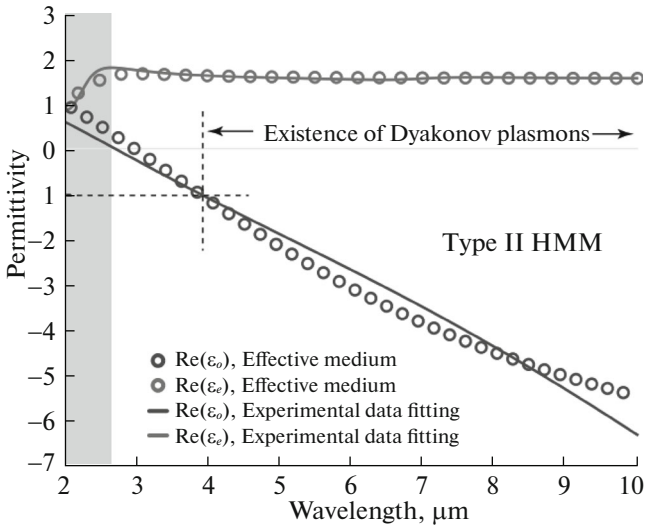

Fig. 2. Dependence of ordinary and extraordinary components of the dielectric function of the AZO/Air trench structure. Solid lines are obtained by fitting of the experimental data using the Drude-Lorentz model with multiple oscillators. The blue and red circle markers are obtained by fitting of the experimental data using the effective medium approach [see Eq. (3)].

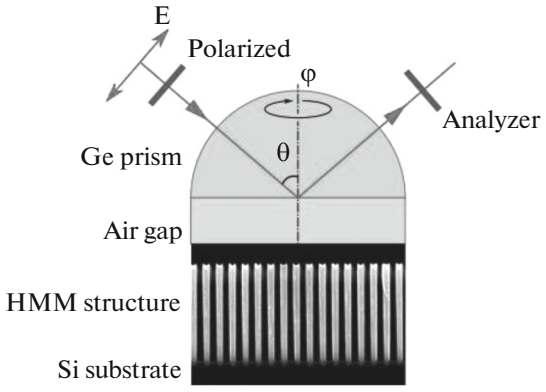

Fig. 3. Scheme of the FTIR experiment setup. The setup provides measurements of the attenuated total reflectance spectra for different incident angles of incident θ and azimuthal angles φ with the use of a Ge prism in the Otto configuration.

Otto configuration of SW excitation. Measurements were conducted at wavelengths $\lambda = 2$–16 μm. Input light was linearly-polarized (TM polarization, magnetic field lies in the *xy* plane, see Fig. 1) and focused on the surface of the structure through the Ge prism. The angle of incidence is θ and the angle between the plane of incidence and the optical axis of the trench structure is φ. Angle θ is manually controlled in the range $\theta = 20°$–$74°$ with a precision about 3° using a goniometer. The divergence angle of the input beam was ±1.7°. The sample orientation with respect to the incident plane (angle φ) is controlled in the range 0°–90° with the step 3°. We measured a series of reflectance spectra at wavelengths $\lambda = 4, 6, 8, 14$ μm varying angles θ and φ. The thickness of the air gap between the prism and trench structure was about 0.5 μm. It was estimated by the best matching between the simulated and measured reflectance spectra.

4. RESULTS AND DISCUSSION

The top row of Fig. 4 shows the experimental TM-polarized reflectance maps for the AZO/Air trench structure at $\lambda = 4, 6, 8, 14$ μm plotted in the Fourier plane (k_x–k_y). The axes for each map are normalized to the wavenumber in vacuum (k_0). Thus, dips in reflection beyond the unit circle (light circle) correspond to the excitation of surface or bulk modes of the structure. Excitation of SWs is evident for the wavelengths $\lambda = 6, 8, 14$ μm in agreement with the DPs existence condition: $|\varepsilon_o| > 1$ (see Fig. 2) [35]. One can see that DPs exist in a broadband spectral range.

The bottom row of Fig. 4 shows the simulated reflectance maps of the AZO/Air trench structure at $\lambda = 4, 6, 8, 14$ μm. One can see that the experimental and simulated maps are in good agreement. The simulations are carried out using the transfer matrix method [36, 37], where the real AZO/Air trench structure is substituted by the effective anisotropic medium with ε_o and ε_e (see Fig. 2) extracted from the experimental reflectance spectra. It is clearly seen from Fig. 4 that as the wavelength increases, the size of the dip corresponding to excitation of DP increases. It is explained by increase of the exponential tails penetrating into the air gap between the prism and sample leading to larger radiative losses. The experimental and simulated reflectance maps also show a secondary mode, most visible at $\lambda = 6, 8$ μm. This mode corresponds to the bulk plasmon polariton (BPP) [38, 39]. BPPs are also known as Langmuir modes [40–43].

AZO has large intrinsic losses making the dips in the reflectance maps broad. To provide more detailed theoretical analysis of the mode structure in air/AZO trenches we reduced the losses by 100 times. The resulting reflectance maps for the TM- and TE-polarized incident waves are shown in Fig. 5. At $\lambda = 4$ μm, the main mode is predominantly TM-polarized and it propagates in a narrow angular domain close to k_y. Thus, we can consider this mode being almost a pure SPP. At $\lambda = 6$ μm the mode becomes hybrid, appearing in both TM- and TE-polarizations. It is a characteristic feature of DPs caused by the anisotropy inherent to HMM [17, 44]. Because of this shape, the DPs exist in a large range of propagation angles in contrary to conventional DWs. The isofrequency contours for DPs become flatter with increase of the wavelength and, as a result, the angular domain of allowed propagation directions becomes broader. The same trend can also be seen in the experimental reflectance maps in Fig. 4. The simulated reflectance maps also show a

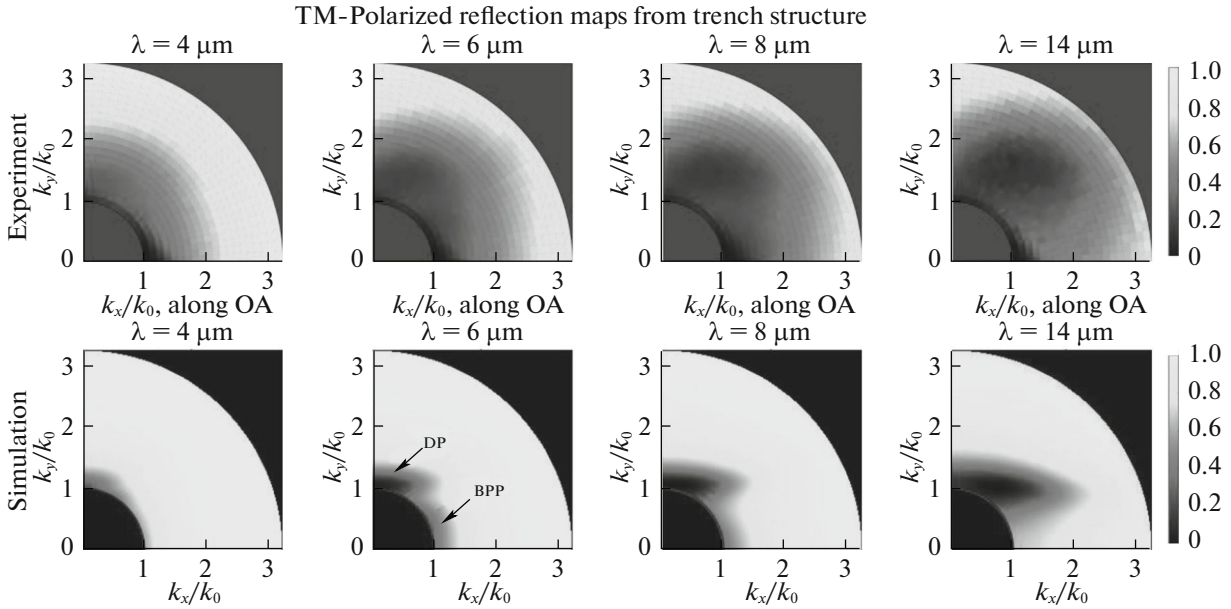

Fig. 4. (top row) Experimental and (bottom row) simulated reflectance maps from AZO/Air trench structure for TM-polarized light: (1st column) 4 μm, (2nd column) 6 μm, (3rd column) 8 μm, (4th column) 14 μm.

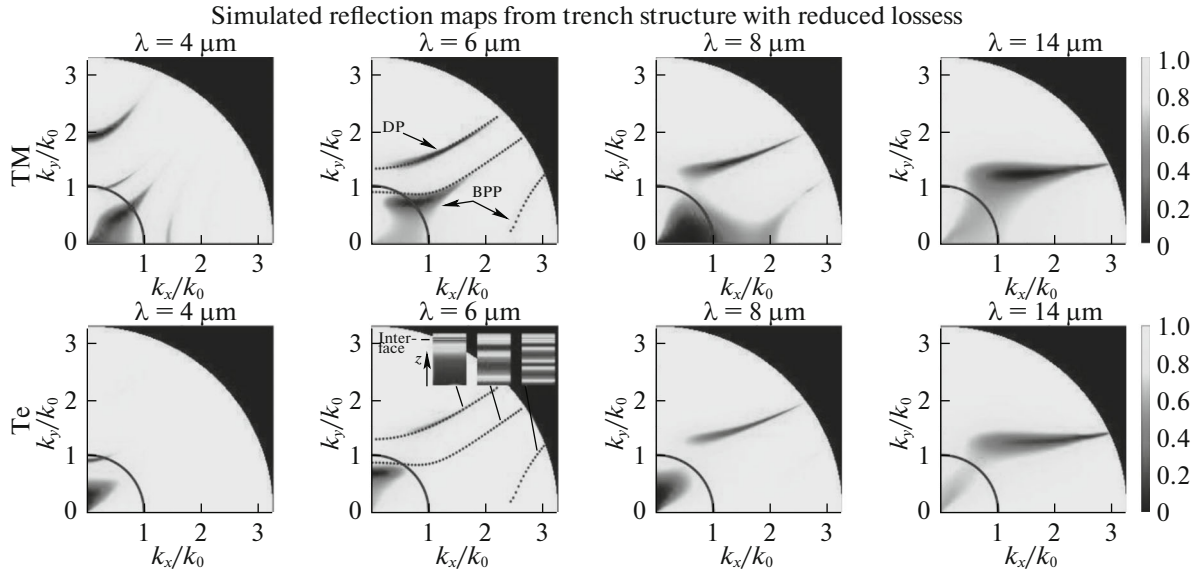

Fig. 5. (top row) Simulated TM- and (bottom row) TE-polarized reflectance maps from AZO/Air trench structure with losses reduced by 100 times: (1st column) 4 μm; (2nd column) 6 μm; (3rd column) 8 μm; (4th column) 14 μm. Blue dot lines are dispersion of eigenmodes calculated in Comsol Multiphysics software. The insets show the distribution of E_x component for Dyakonov plasmon and bulk plasmon polaritons.

number of nearly pure TM-polarized modes, which correspond to BPPs. With increasing wavelength, the number of supported BPP modes decreases. Therefore, the density of optical states in the system under consideration strongly depends on the wavelength and it is maximal at $\lambda \approx 4$ μm (see Fig. 2). To confirm the simultaneous presence of DP and BPPs in the spectrum we modelled eigenmodes and their field distributions with the Comsol Multiphysics. The dispersion of the eigenmodes are shown with blue dot lines in Fig. 5. The field mapping of the E_x component shown in the insets of Fig. 5 confirms excitation of DP and BPPs.

5. CONCLUSIONS

In conclusion, we experimentally confirmed excitation of Dyakonov plasmons in a wide wavelength range in mid-IR. Necessary anisotropy was provided

by the structure consisting of vertical alternating layers of AZO and air. All steps in fabrication are supported by large-scale CMOS compatible highly reproducible technological processes. Flexibility of the optical properties of the analyzed structures makes them very prospective for a plethora applications in nanophotonics and biosensing. The obtained results provide useful guidelines for practical implementations of structures supporting Dyakonov plasmons in the mid-IR.

ACKNOWLEDGMENTS

This work was supported by VillumFonden Dark-SILD" project no. 11116, the Russian Foundation for Basic Research (16-37-60064, 17-02-01234, 16-32-00248), the Ministry of Education and Science of the Russian Federation (3.1668.2017/4.6), the President of Russian Federation (MK-403.2018.2).

REFERENCES

1. J. A. Polo and A. Lakhtakia, Laser Photon. Rev. **5**, 234 (2011)
2. A. V. Kildishev, A. Boltasseva, and V. M. Shalaev, Science (Washington, DC, U. S.) **339** (6125), 1232009 (2013)
3. O. Takayama, A. A. Bogdanov, and A. V. Lavrinenko, J. Phys.: Condens. Matter **29**, 463001 (2017).
4. J. Homola, Anal. Bioanal. Chem. **377**, 528 (2003).
5. M. Righini, G. Volpe, C. Girard, D. Petrov, and R. Quidant, Phys. Rev. Lett. **100**, 186804 (2008).
6. S. Kawata, Y. Inouye, and P. Verma, Nat. Photon. **3**, 388 (2009).
7. W. L. Barnes, A. Dereux, and T. W. Ebbesen, Nature (London, U.K.) **424** (6950), 824 (2003).
8. D. K. Gramotnev and S. I. Bozhevolnyi, Nat. Photon. **8**, 13 (2014).
9. R. W. Wood, Philos. Mag. **4**, 396 (1902).
10. S. A. Maier, M. L. Brongersma, P. G. Kik, S. Meltzer, A. A. Requicha, and H. A. Atwater, Adv. Mater. **13**, 1501 (2001).
11. H. A. Atwater and A. Polman, Nat. Mater. **9**, 205 (2010).
12. M. Dyakonov, Sov. Phys. JETP **67**, 714 (1988).
13. O. Takayama, L. C. Crasovan, S. K. Johansen, D. Mihalache, D. Artigas, and L. Torner, Electromagnetics **28**, 126 (2008).
14. O. Takayama, L. Crasovan, D. Artigas, and L. Torner, Phys. Rev. Lett. **102**, 043903 (2009).
15. O. Takayama, D. Artigas, and L. Torner, Nat. Nanotechnol. **9**, 419 (2014).
16. D. Artigas and L. Torner, Phys. Rev. Lett. **94**, 013901 (2005).
17. Z. Jacob and E. E. Narimanov, Appl. Phys. Lett. **93**, 221109 (2008).
18. I. Avrutsky, I. Salakhutdinov, J. Elser, and V. Podolskiy, Phys. Rev. B **75**, 241402 (2007).
19. H. N. Krishnamoorthy, Z. Jacob, E. Narimanov, I. Kretzschmar, and V. M. Menon, Science (Washington, DC, U. S.) **336** (6078), 205 (2012).
20. S. Ishii, A. V. Kildishev, E. Narimanov, V. M. Shalaev, and V. P. Drachev, Laser Photon. Rev. **7**, 265 (2013)
21. G. V. Naik, B. Saha, J. Liu, S. M. Saber, E. A. Stach, J. M. Irudayaraj, T. D. Sands, V. M. Shalaev, and A. Boltasseva, Proc. Natl. Acad. Sci. USA **111**, 7546 (2014)
22. K. V. Sreekanth, Y. Alapan, M. ElKabbash, E. Ilker, M. Hinczewski, U. A. Gurkan, A. de Luca, and G. Strangi, Nat. Mater. **15**, 621 (2016)
23. R. Maas, J. Parsons, N. Engheta, and A. Polman, Nat. Photon. **7**, 907 (2013)
24. A. A. High, R. C. Devlin, A. Dibos, M. Polking, D. S. Wild, J. Perczel, N. P. de Leon, M. D. Lukin, and H. Park, Nature (London, U.K.) **522** (7555), 192 (2015)
25. M. Noginov, Y. A. Barnakov, G. Zhu, T. Tumkur, H. Li, and E. Narimanov, Appl. Phys. Lett. **94**, 151105 (2009)
26. A. Kabashin, P. Evans, S. Pastkovsky, W. Hendren, G. Wurtz, R. Atkinson, R. Pollard, V. Podolskiy, and A. Zayats, Nat. Mater. **8**, 867 (2009)
27. C. T. Riley, J. S. Smalley, K. W. Post, D. N. Basov, Y. Fainman, D. Wang, Z. Liu, and D. J. Sirbuly, Small **12**, 892 (2016).
28. P. R. West, S. Ishii, G. V. Naik, N. K. Emani, V. M. Shalaev, and A. Boltasseva, Laser Photon. Rev. **4**, 795 (2010).
29. G. V. Naik, J. Kim, and A. Boltasseva, Opt. Mater. Express **1**, 1090 (2011).
30. Y. Zhong, S. D. Malagari, T. Hamilton, and D. M. Wasserman, J. Nanophoton. **9**, 093791 (2015).
31. J. A. Dionne, K. Diest, L. A. Sweatlock, and H. A. Atwater, Nano Lett. **9**, 897 (2009).
32. E. Shkondin, O. Takayama, J. M. Lindhard, P. V. Larsen, M. D. Mar, F. Jensen, and A. V. Lavrinenko, J. Vac. Sci. Technol., A **34**, 031605 (2016).
33. E. Shkondin, O. Takayama, M. A. Panah, P. Liu, P. V. Larsen, M. D. Mar, F. Jensen, and A. Lavrinenko, Opt. Mater. Express **7**, 1606 (2017).
34. V. Agranovich and V. Kravtsov, Solid State Commun. **55**, 85 (1985).
35. O. Takayama, D. Artigas, and L. Torner, Opt. Lett. **37**, 4311 (2012).
36. P. Yeh, Surf. Sci. **96**, 41 (1980).
37. P. Dmitriev, kitchenknif/pyatmm, V1.0.0-a1 (2017). https://doi.org/10.5281/zenodo.1041040
38. O. Takayama, E. Shkondin, A. Bogdanov, M. E. Aryaee Pahah, K. Golenitskii, P. A. Dmitriev, T. Repan, R. Malreanu, P. Belov, F. Jensen, and A. Lavrinenko, ACS Photon. (2017, in press)
39. N. Vasilantonakis, M. E. Nasir, W. Dickson, G. A. Wurtz, and A. V. Zayats, Laser Photon. Rev. **9**, 345 (2015)
40. A. A. Bogdanov and R. A. Suris, JETP Lett. **96**, 49 (2012)
41. K. Y. Golenitskii, K. L. Koshelev, and A. A. Bogdanov, Phys. Rev. A **94**, 043815 (2016)
42. K. L. Koshelev and A. A. Bogdanov, Phys. Rev. B **94**, 115439 (2016)
43. K. L. Koshelev and A. A. Bogdanov, Phys. Rev. B **92**, 85305 (2015).
44. O. Y. Yermakov, A. I. Ovcharenko, M. Song, A. A. Bogdanov, I. V. Iorsh, and Y. S. Kivshar, Phys. Rev. B **91**, 235423 (2015)